

Magnetic Field Sensing with 4H SiC Diodes: N vs P Implantation

Corey J. Cochrane^{1,a*}, Hannes Kraus^{1,b}, Philip G. Neudeck^{2,c}, David Spry^{2,d},
Ryan J. Waskiewicz^{3,e}, James Ashton^{3,f} Patrick M. Lenahan^{3,g}

¹Jet Propulsion Laboratory, California Institute of Technology, Pasadena, CA 91109, USA

²NASA Glenn Research Center, Cleveland, OH 44135, USA

³The Pennsylvania State University, University Park, PA 16802, USA

^acorey.j.cochrane@jpl.nasa.gov, ^bhannes.kraus@jpl.nasa.gov, ^cneudeck@nasa.gov,
^ddavid.j.spry@nasa.gov, ^erjw5352@psu.edu, ^fjpa5108@psu.edu, ^gpmlesm@engr.psu.edu

Keywords: magnetometer, magnetoresistance, atomic scale defects, spin dependent recombination, electrically detected magnetic resonance, silicon carbide

Abstract: We explore the magnetic sensing capabilities of two 4H-SiC n⁺p diodes fabricated by NASA Glenn which only differ in the implanted ion species, nitrogen and phosphorus, and the implant activation annealing time. We use low- and high-field electrically detected magnetic resonance (EDMR) to investigate the defect structure used to sense magnetic fields as well as to evaluate the sensitivity. In addition, we expose these devices to high energy electron radiation to evaluate the defect sensing capability in a harsh radiation environment. The results from this work will allow us to tailor our processing methods to design a more optimal 4H-SiC pn diode for magnetic field sensing in harsh environments.

Introduction

The idea of facilitating the magnetic resonance properties of spin-carrying quantum centers in solid state materials for the detection of magnetic fields has been around for some time. Theoretical considerations [1] led to first proof-of-concept magnetometry via optically detected magnetic resonance (ODMR) on NV centers in diamond [2,3]. Although the diamond/ODMR approach shows promise, it is—due to the nature of diamond [4]—not feasible for integration into an electrical device. However, the more electrically accessible silicon carbide was shown to carry a similar class of quantum defects [5], also with a lot of promise for magnetometry application [6-8].

Electrical readout of similar quantum centers has even been shown to be accessible in fully processed 4H-SiC devices by measuring small changes in current associated with resonant (EDMR) and non-resonant (zero-field mixing) spin dependent recombination (SDR) [9]. Over the last couple years, we've reported on the initial stages of development of a solid-state magnetometer which leverages this phenomenon as the field-sensing mechanism [10,11]. The magnetometer previously used the source/drain pn junction region of an experimental 4H SiC MOSFET (P-implant, gate area 400x400 μm^2) which was characterized with a magnetic field sensing sensitivity of about 400 nT/ $\sqrt{\text{Hz}}$ [11]. As this device is not ideal for space applications due to the presence of an oxide which has the potential to accumulate charge from electron and ion radiation sources, we are now in the process of designing a custom sensor with simple 4H-SiC vertical pn junction diode structures. However, prior to design and fabrication of these custom devices, much investigation into the influence of the processing needs to be evaluated to optimize for sensitivity. The sensitivity metric is based on that reported in Cochrane 2016 [11], $\delta B/\sqrt{\Delta f} = 2\sigma\sqrt{\pi q I_0}/\Delta I$ (T/ $\sqrt{\text{Hz}}$). Here, σ is the linewidth of the signal, q is the electronic charge, and Δf is the bandwidth of measurement. In this work, we look to evaluate one of the key trade parameters, that being the effect of the ion implantation species used for doping the SiC semiconductor. Here, we evaluate the magnetic field sensing capability of two sets of nearly identical n+p diodes fabricated at NASA Glenn. The 250 μm diameter diodes were formed by the same high-dose n-type implantations used to make source/drain regions for two different JFET IC wafer runs, contacted by a 162 μm diameter IrIS metal stack [12-14]. The major difference between the two sets of diodes is that one received a nitrogen (N) implant with a 4 hour activation annealing time while the other a phosphorus (P) implant with a ~100 hour activation

annealing time. We leverage the spectroscopic technique of low-field ($B_0 \sim 8.9 \text{ mT}$, $\nu \sim 250 \text{ MHz}$) and high-field ($B_0 \sim 339 \text{ mT}$, $\nu \sim 9.5 \text{ GHz}$) electrically detected magnetic resonance (EDMR), to investigate the deep-level defects responsible for SDR in the N- and P-implanted diodes. The low-field technique not only allows us to observe the resonance of the electrons tied up in the defects, but also allows us to simultaneously observe the magnetoresistive response, which we refer to as zero-field SDR; which is the basis of the operation of the magnetometer in development.

EDMR Results on As Processed Devices

Figure 1 illustrates the data gathered on the N-implanted diode. Figure 1a represents a low-field measurement with the zero-field (0 mT) and resonant SDR (8.9 mT) signals present. Note the hyperfine structure in both signals indicated by the black arrows. Figures 1b and 1c illustrate a better resolved low-field EDMR response (0.15 mT modulation) with the B_0 field parallel and perpendicular to the crystalline c-axis, respectively. Note that the spacing between the hyperfine peaks reduces from 1.3 mT to 1.04 mT when the sample is rotated with respect to applied magnetic field. Figure 1d illustrates the change in the integrated zero-field SDR current ΔI and the DC current I_0 as a function of applied bias. Using the sensitivity metric reported in [11], the highest sensitivity of the N-implanted devices is about $1000 \text{ nT}/\sqrt{\text{Hz}}$ when biased with 6.5 V . (The smaller sensitivity compared to the MOSFET is tentatively attributed to the smaller sensing area of the diode used in this study.)

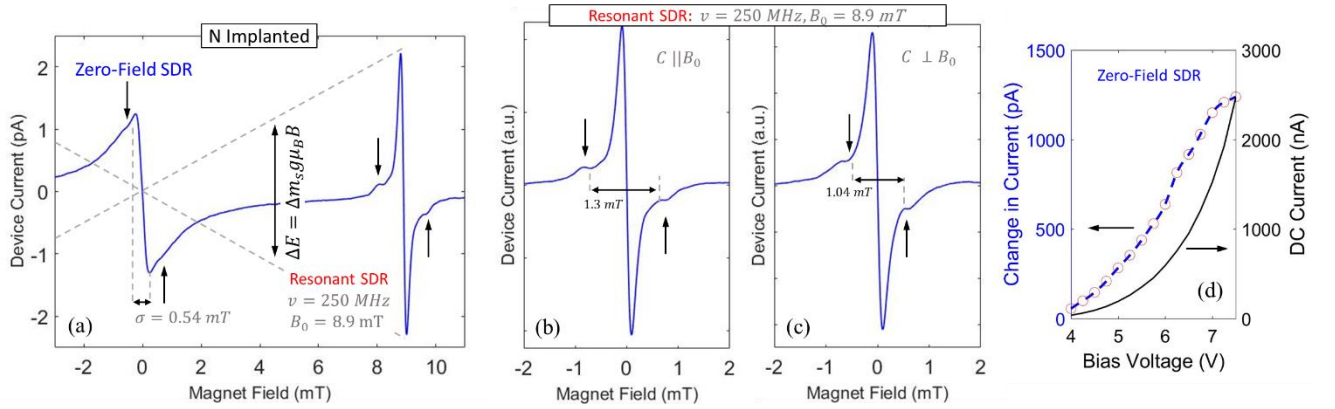


Figure 1: Data from N-implanted diode. (a) Low-field EDMR spectrum illustrating both zero-field and resonant SDR responses. Low-field EDMR spectrum with (b) B_0 parallel to the crystalline c-axis and (c) with B_0 perpendicular to the crystalline c-axis. (d) Change in the integrated zero-field SDR current and DC current as a function of applied bias. (Note that signal is too weak to measure below 4 V and too noisy above 7.5 V)

Figure 2 illustrates similar measurements on the P-implanted device. When comparing the two data sets, there are two main important differences. The first noticeable difference is that even though the dominant defect appears to be the same in both devices, there appears to be an additional set of more pronounced hyperfine side peaks in the P-implanted device as illustrated by the red arrows in Figure 2a and 2b. These side peaks are spaced about 0.75 mT apart when the B_0 field is parallel to the crystalline c-axis and disappear into the central line when rotated 90° . It is likely that these additional side peaks are due to a secondary defect involving a complex coupled to a neighboring $I = 1/2$ phosphorous atom. The other noticeable difference between the two data sets is that both the change in integrated zero-field current ΔI and DC current I_0 are significantly lower for the P-implanted devices, suggesting that there are fewer defects that contribute to recombination. In fact, the highest sensitivity measured for the P-implanted devices was about $5000 \text{ nT}/\sqrt{\text{Hz}}$ with 5 V applied to the junction.

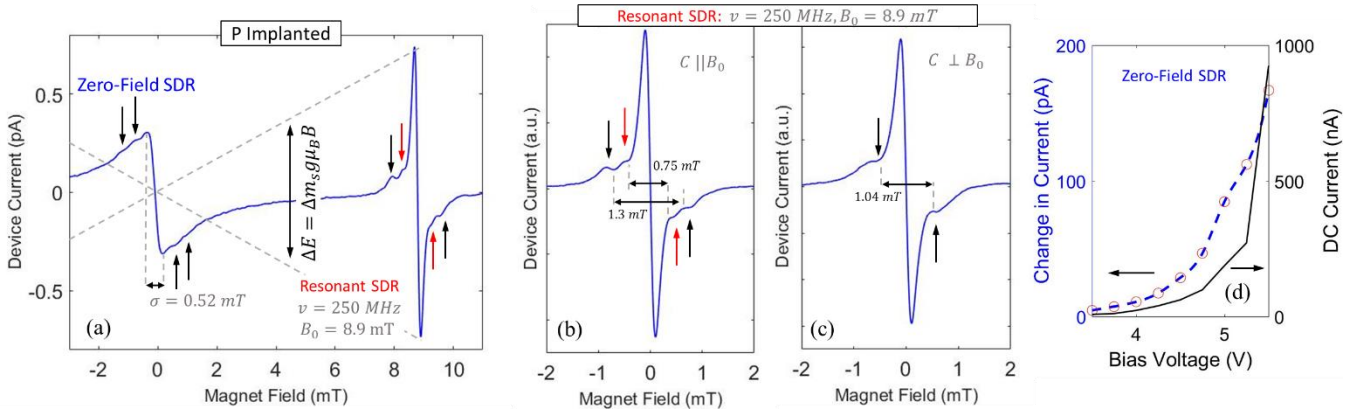


Figure 2: Data from P-implanted diode. (a) Low-field EDMR spectrum illustrating both zero-field and resonant SDR responses. Low-field EDMR spectrum with (b) B_0 parallel to the crystalline c-axis and (c) with B_0 perpendicular to the crystalline c-axis. (d) Change in the integrated zero-field SDR current and DC current as a function of applied bias. (Note that signal is too weak to measure below 3.5V and too noisy above 5.5V)

As it is very difficult to obtain precise g values in the low-field measurements due to the loss in resolution, high-field measurements (X-Band) were performed to more precisely investigate the orientation dependence of the g and hyperfine parameters of the defect under observation. Figure 3 illustrates the X-band EDMR on both N- and P-implanted devices with the crystalline-c axis oriented parallel and perpendicular to the applied magnetic field. The clear difference between these measurements (9.5 GHz) and their associated low-field measurement (0.25 GHz) is that the N-doped devices appears significantly broadened at X-band, which we attribute to a higher level of disorder around the defects. This result is not surprising considering the N-doped devices are significantly more damaged than the P-doped devices. Additionally, the X-band measurements corroborate the anisotropic nature of the hyperfine interactions observed in the low-field measurements (although broadened in the N-doped case). In both cases, the dominant center line is characterized as having an isotropic $g \approx 2.0029 \pm 0.0001$ which is consistent with a silicon vacancy [15].

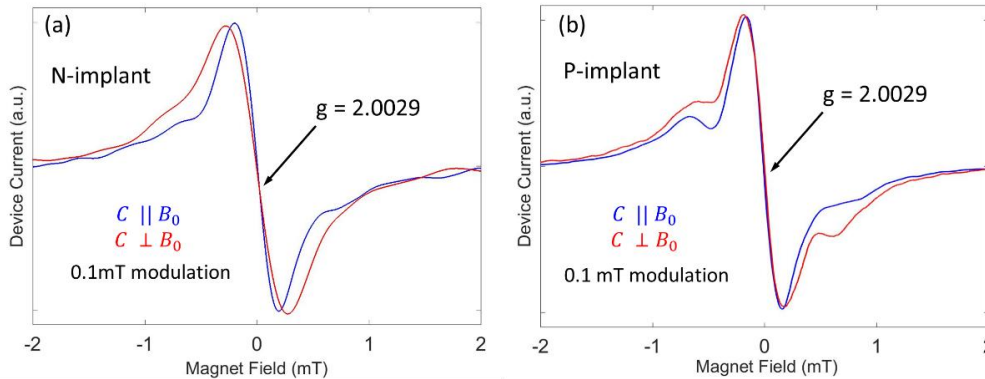


Figure 3: X-band EDMR data obtained from (a) N- and (b) P-implanted diodes with their crystalline c-axis orientated parallel and perpendicular to the applied magnetic field.

EDMR Results on Electron Irradiated Devices

In order for the sensor to operate reliably in space and harsh planetary environments, it needs to be able to withstand radiation doses in excess 10^7 's of Mrad. In order to test the sensors performance in an analogous environment, we leveraged JPL's Dynamitron electron irradiation facility to expose the sensors to comparable electron doses (fluence of 1×10^{14} e/cm^2 , energy of 2 MeV) with both contacts of the diodes tied to a common ground. Figure 4 compares the DC current I_0 , change in current ΔI (integrated raw data), and approximate sensitivity δB versus the applied junction bias for both irradiated and non-irradiated devices. As illustrated in the figure, it appears that for both N- and P-doped irradiated devices, a smaller junction bias is required to achieve the same DC current I_0 and change in SDR current ΔI (and hence δB). This result clearly indicates that the built-in voltage of the diodes is reduced after exposure to the high-energy electrons. Note however that the optimum

sensitivity is unaffected in each device, although a slightly smaller bias is required to achieve the same metric. These results demonstrate the robustness of the SiC sensor as a magnetic field sensing device with much promise for harsh radiation environments.

It should be noted that the devices presented in this study were not originally designed in any way for magnetometry. The defects detected via EDMR were those intrinsic to the device after ion implantation. Our next step is to design and fabricate diodes of various sizes, geometry, annealing, and doping species/concentration to experimentally ascertain the magnetic field sensing capability of larger variety of implant processes. Additionally, defect engineering practices will be used to better tailor the defects to help meet our sensitivity goal of $1 \text{ nT}/\sqrt{\text{Hz}}$.

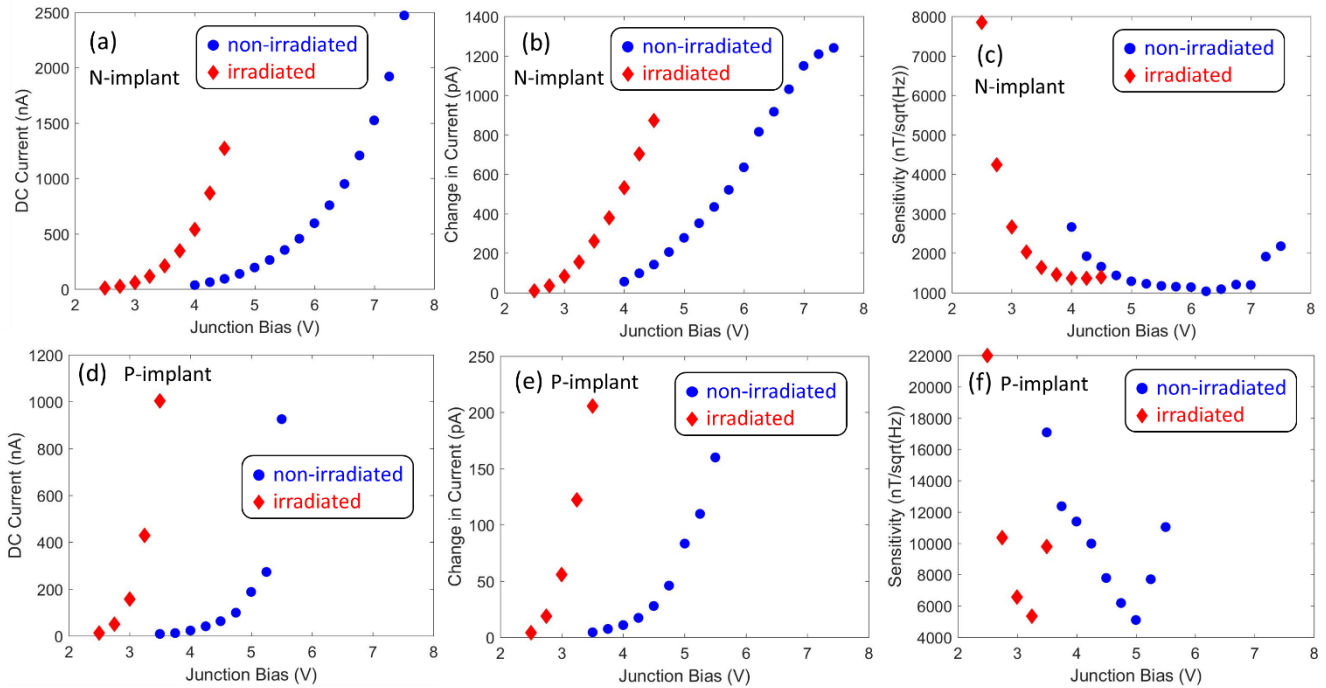


Figure 4: Comparison of DC current I , change in current ΔI , and sensitivity δB as a function of applied bias for non-irradiated and irradiated (a-c) N implanted and (d-f) P implanted 4H SiC diodes.

Summary

These measurements demonstrate that the “as processed” nitrogen-implanted 4H-SiC diodes are plagued with more atomic scale defects than identical structures implanted with phosphorous, a result that the fabrication and reliability communities may find of significant interest. While the implant anneals were substantially different, this initial result suggests that the N-implanted diodes may be better suited for magnetic field sensing applications. In addition, data obtained from exposure to electron radiation similar to that encountered in a planetary system such as Jupiter indicate that minimal degradation to magnetometer performance is achieved over the anticipated mission lifetime of the sensor.

Acknowledgement

The research described here was carried out at the Jet Propulsion Laboratory, California Institute of Technology, under a contract with the National Aeronautics and Space Administration., supported by PICASSO. Device fabrication at NASA Glenn Research Center was supported by both PICASSO and the NASA Aeronautics Transformative Technologies and Tools project.

References

- [1] B. Chernobrod and G. Berman, *J. Appl. Phys.* 97, 1, (2005).
- [2] J. R. Maze, et al., *Nature* 455, 7213, 644–647 (2008).
- [3] K. Balasubramanian, et al., *Nature* 455, 7213, 648–651 (2008)
- [4] R. Kalish, *Carbon* 37, 5, 781–785 (1999).
- [5] D. Riedel, et al., *Phys. Rev. Lett.* 109, 22, 226402 (2012).
- [6] H. Kraus, V. A. Soltamov, et al., *Sci. Rep.* 4 5303 (2014).
- [7] D. Simin, et al., *Phys. Rev. Appl.* 4, 1, 014009–8 (2015).
- [8] M. Niethammer, et al., *Phys. Rev. Applied* 6, 3, (2016).
- [9] C.J. Cochrane, et al., *J Appl. Phys.* 112, 123714 (2012).
- [10] C. J. Cochrane, et al., *Mat. Sci. For.*, 858, 265-268, (2016).
- [11] C. J. Cochrane, et al., *Sci. Rep.* 6, 1, 1239 (2016).
- [12] D. J. Spry, et al., *Mat. Sci. For.* 828 908-912 (2016)
- [13] D. J. Spry, et al., *IEEE Elec. Dev. Lett.* 38 1082-1085 (2017).
- [14] D. J. Spry, D. Lukco, *J. Electron. Mater.* 41 915-920 (2012).
- [15] C. J. Cochrane, et al., *Appl. Phys. Lett.* 100, 023509 (2012).